J. Appl. Comput. Mech., xx(x) (2026) 1-8
DOI: 10.22055/jacm.2026.49691.6165

ISSN: 2383-4536
jacm.scu.ac.ir

Shahid Chamran University of Ahvaz

Journal of Applied and Computational Mechanics



Research Paper

Event-Driven Asymptotic Continuation and Regular Branch Decomposition for Signorini Contact

Mohamed Hamdaoui

Université de Lorraine, LEM3, UMR CNRS 7239, 7 rue Félix Savart, 57070 Metz, France, Email: mohamed.hamdaoui@univ-lorraine.fr

Received August 09 2026; Revised October 07 2026; Accepted for publication October 07 2026.
✉ Corresponding author: M. Hamdaoui (mohamed.hamdaoui@univ-lorraine.fr)
© 2026 Published by Shahid Chamran University of Ahvaz

Abstract. Opening or closing a unilateral contact changes the smooth equilibrium equations followed by a continuation method. We combine high-order asymptotic numerical continuation on a fixed contact stratum with nonlinear correction of the predicted event to one common state, followed by support-based classification of regular outgoing branches. The local existence argument is standard; the contribution is the event-driven organization of feasible support rays, shared tangent reduction, and separation of branch existence from traversal direction. In a symmetric seven-node truss, a simultaneous two-contact opening gives three forward branches. A sparse finite-element strip confirms transfer to assembled systems. The results concern quasistatic, frictionless contact with fixed normals and regular one- or two-contact events.

Keywords: Signorini contact; asymptotic numerical method; nonlinear continuation; complementarity; branch switching; finite element method.

1. Introduction

With unilateral contact, a continuation path is smooth only while the contact status remains unchanged. An open gap may close, or an active normal reaction may fall to zero; at that instant the set of equality constraints changes. Several admissible contact statuses can also meet at the same equilibrium. We therefore keep three questions separate: where the event is located, which local branches actually leave it, and which of those branches should be followed in the chosen continuation direction.

High-order asymptotic numerical methods (ANM) provide efficient continuation on smooth equilibrium strata [1–3]. ANM predictor–corrector formulations have also been developed for unilateral contact [4–6]. In parallel, contact mechanics has a substantial literature on critical points, branch switching, unilateral constraints and nonsmooth continuation [7–13]. More recent work continues to emphasize robust continuation control and the algorithm dependence that may arise in multiple-solution contact calculations [14, 15].

Recent finite-element work on Signorini-type models has concentrated mainly on approximation and error control in coupled settings, including piezoelectric, thermoelastic, frictional and curved-boundary problems [16–19]. Two further studies consider a penalized Coulomb-frictional Signorini problem for locking piezoelectric materials and a thermo-electro-elastic Lamé system with penalized contact conditions [20, 21]. Those papers are concerned with penalization, finite-element approximation, and convergence or error estimates. Our question is different: how to continue an equilibrium path through a change of active contact set and how to identify the regular local branches that leave the corrected event. The two lines of work are complementary.

We do not present Theorem 1 as a new general existence theorem; its implicit-function-theorem argument is standard. The contribution is the way this local result is organized around a corrected contact event. The same nonlinear event state is used for every candidate support. Each support is then tested for a feasible regular ray, and those rays identify the regular strictly complementary half-branch germs covered by the theorem. The large mechanical part of the tangent problem is reused through a low-dimensional reduction, with a direct outgoing solve retained as a fallback. Only after a branch has been shown to exist is it labelled forward or reverse for continuation.

The two examples answer different questions. The seven-node truss is deliberately small, so every support choice and every local branch at the critical junction can be inspected. The twin-pad finite-element strip asks whether the same event treatment can be used once the mechanical equations come from a sparse finite-element assembly. It is an engineering transfer test, not a continuum-convergence study and not evidence for a new physical bifurcation. Both configurations are shown in Fig. 1.

1.1. Scope and computational scaling

The demonstrated analysis assumes fixed candidate nodes, fixed normals, frictionless quasistatic Signorini contact, regular outgoing strata, strict first-order complementarity, and accepted event groups containing one or two contacts. Grazing, higher-order departure, singular strata, friction, closest-point updates and changing normals are outside the theorem. For an event group of size $k = |\mathcal{E}|$, exhaustive support classification tests 2^k supports.

Published online: November 05 2026

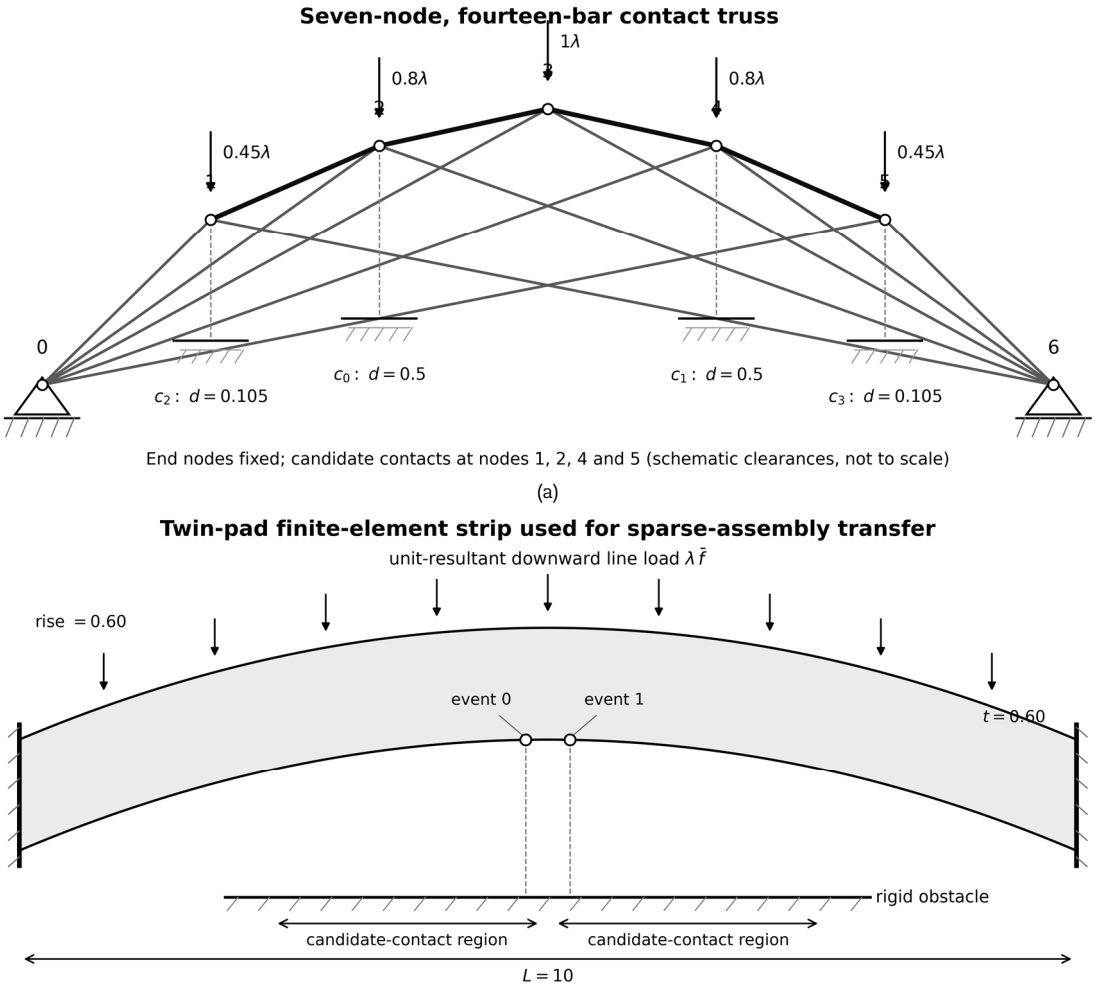


Fig. 1. Engineering configurations used in the study: (a) seven-node, fourteen-bar contact truss with four candidate vertical contacts; (b) geometrically nonlinear twin-pad finite-element strip above a rigid obstacle. Clearances and pad separation are schematic.

The common reduction reuses the large mechanical factorization, but it does not remove this exponential combinatorial growth; the method is therefore intended as a transparent classifier for small simultaneous groups rather than a scalable enumeration strategy for large k. Five decisive truss segments receive computer-assisted exclusion of earlier contact zeros; the remainder of the operational graph is numerically re-stepped but not interval certified.

2. From a Smooth Stratum to a Corrected Event

2.1. Terminology and discrete Signorini strata

In this paper, an equilibrium path is simply a curve of balanced mechanical states as the load changes. A contact event is reached when an open gap closes or an active contact force drops to zero. ANM provides a high-order prediction of that point, but the polynomial root is not used as the final event state. We call corrected event the nearby state that satisfies the full nonlinear equilibrium equations together with the event condition. A support then specifies which of the event contacts are active just after the event, and a branch is a local equilibrium curve compatible with that choice.

Let $\mathbf{u} \in \mathbb{R}^n$ be the displacement vector, $\lambda \in \mathbb{R}$ the load factor, and $\mathbf{p} \in \mathbb{R}^m$ the compressive normal contact multipliers. With external load vector $\mathbf{f}$, fixed contact operator $\mathbf{B}$, and clearance vector $\mathbf{d}$:

$$\mathbf{R}(\mathbf{u}, \lambda, \mathbf{p}) = \mathbf{f}_{\text{int}}(\mathbf{u}) - \lambda \mathbf{f} + \mathbf{B}^T \mathbf{p} = \mathbf{0}. \tag{1}$$

$$\mathbf{g}(\mathbf{u}) = \mathbf{d} - \mathbf{B}\mathbf{u}. \tag{2}$$

The Signorini conditions are:

$$\mathbf{g} \geq \mathbf{0}, \qquad \mathbf{p} \geq \mathbf{0}, \qquad \mathbf{g} \odot \mathbf{p} = \mathbf{0}. \tag{3}$$

with $\mathbf{y} = (\mathbf{u}, \lambda, \mathbf{p})$ and $\mathcal{I} = \{1, \ldots, m\} \setminus \mathcal{A}$, an active set $\mathcal{A}$ selects the smooth equality system:

$$\mathbf{F}_{\mathcal{A}}(\mathbf{y}) = \begin{bmatrix} \mathbf{R}(\mathbf{u}, \lambda, \mathbf{p}) \\ -\mathbf{g}_{\mathcal{A}}(\mathbf{u}) \\ \mathbf{p}_{\mathcal{I}} \end{bmatrix} = \mathbf{0}. \tag{4}$$

Table 1. Principal numerical thresholds used for the truss benchmark.

Role	Test	Value
Corrected-state promotion	$\lvert h_i\rvert \le \tau_{\text{promote}}$	5×10^{-13}
Common event correction	block ℓ_∞ residuals	5×10^{-13}
Non-event separation	minimum gap or multiplier	2×10^{-10}
Transversality	$\lvert Dh_i(\mathbf{y}_e)\mathbf{c}_e\rvert$	10^{-10}
Rank	relative singular-value threshold	10^{-12}
Ray feasibility	minimum strict event rate	2×10^{-10}

On the interior of this stratum, active multipliers and inactive gaps are positive. A contact event occurs when one or more of these strict inequalities reaches zero. The analytical notation uses contact indices $1, \dots, m$; the implementation and benchmark tables use zero-based contact labels, which are identified explicitly where they appear.

2.2. ANM predictor on one stratum

At a regular point $\mathbf{y}_0$, ANM represents the nearby path as:

$$\mathbf{y}(a) = \mathbf{y}_0 + \sum_{k=1}^{P} a^k \mathbf{y}_k, \qquad \mathbf{c}^T\mathbf{M}(\mathbf{y}(a) - \mathbf{y}_0) = a, \tag{5}$$

where $\mathbf{M}$ is a positive-definite continuation metric and $\mathbf{c}$ is the metric-unit tangent. The active multipliers and inactive gaps are evaluated along the same Taylor series; positive real zeros provide event candidates. Numerical coefficient filtering, root isolation and near-start handling are used only to produce and localize a candidate. A grazing or near-multiple root that cannot be shown transversal is returned as unresolved. The earliest retained root therefore predicts where the current smooth stratum may end; it does not define the corrected event state or establish simultaneity.

2.3. Common-state correction and acceptance

Prediction and correction play different roles. The ANM root supplies a nearby initial guess; the nonlinear corrector determines the event state used for mechanics and branch classification. Let $\mathcal{A}^-$ be the incident active set and $\mathcal{E}$ a proposed event group. Write $h_i = g_i$ for a closure and $h_i = p_i$ for an opening. Starting from the polynomial predictor, the corrected event state $\mathbf{y}_e$ satisfies:

$$\mathcal{C}_{\mathcal{E}}(\mathbf{y}_e) = \begin{bmatrix} \mathbf{F}_{\mathcal{A}^-}(\mathbf{y}_e) \\ \{h_i(\mathbf{y}_e)\}_{i\in\mathcal{E}} \end{bmatrix} = \mathbf{0}. \tag{6}$$

The earliest predictor is corrected first. With one event equation, Eq. (6) is square; with two event equations it is overdetermined. In the truss calculations, analytic-Jacobian trust-region least squares is used with Jacobian scaling. Every incident-stratum equation and every event equation must satisfy its own tolerance. Thus a simultaneous event is accepted only when the proposed event coordinates vanish at one common equilibrium state; two nearby polynomial roots are not enough. After each correction, every active multiplier and every inactive gap is reevaluated, including coordinates that did not generate a retained predictor root. Any additional vanishing coordinate is promoted and the enlarged group is corrected again.

Because Eq. (6) does not impose a phase section, the corrected state must remain near the predictor that initiated the solve. For the ANM segment based at $\mathbf{y}_0$ with phase row $\mathbf{c}^T\mathbf{M}$, define the corrected phase coordinate as $a_e = \mathbf{c}^T\mathbf{M}(\mathbf{y}_e - \mathbf{y}_0)$. Let $\mathbf{c}_e$ denote the metric-unit tangent recomputed at $\mathbf{y}_e$ on the incident stratum and oriented in the direction from which the event is approached. It is used for the corrected-state transversality test and later only as a reference orientation for traversal labels. For the predictor interval, write $I_p = [a_{\text{lo}}, a_{\text{hi}}]$ with width $\lvert I_p\rvert = a_{\text{hi}} - a_{\text{lo}}$ and let h'_p be the derivative of the retained event polynomial at the initiating root. With correction tolerance τ_{corr}, transversality threshold τ_{tr}, and segment radius $a_{\max}$, define:

$$\delta_a = \max\left(20\lvert I_p\rvert, \frac{20\tau_{\text{corr}}}{\max(\lvert h'_p\rvert, \tau_{\text{tr}})}, 10^{-8}a_{\max}\right). \tag{7}$$

Acceptance requires $\delta_a \le 0.05 a_{\max}$ and $a_{\text{lo}} - \delta_a \le a_e \le a_{\text{hi}} + \delta_a$. It also requires transversality, full column rank of the correction Jacobian, and strict separation of every non-event coordinate. A failed test returns an unresolved event rather than a forced branch decision.

Table 1 lists the principal nondimensional thresholds used for the truss calculations. Predictor tolerances only localize the nonlinear correction; corrected-state tests determine the event group and branch decision.

Across the 24 accepted graph events, the largest event-block and incident-stratum infinity norms are 9.58×10^{-16} and 1.01×10^{-15}; the smallest scaled multi-event correction singular-value ratio is 4.20×10^{-3}, and the smallest non-event margin is 7.31×10^{-4}. All accepted corrections satisfy the localization test in Eq. (7).

2.4. Computational workflow

Operationally, one continuation segment is handled in a fixed order. First, the current active-set stratum is continued until the earliest event candidate is isolated. The candidate is then corrected with the nonlinear incident-stratum and event equations. All contact coordinates are reevaluated at the corrected state, and the event group is enlarged if another coordinate also vanishes. The supports of the accepted small group are then classified, using the direct outgoing system whenever the common reduction is not reliable. Only after this classification are traversal direction and branch restart decided. If localization, rank, separation or transversality fails, the event is left unresolved rather than forcing a branch choice.

3. Regular Local Branch Decomposition

Once the event has been corrected, the remaining local question is finite and combinatorial. Every event contact is either active or open immediately after the event; two event contacts therefore give four candidate states. For each candidate state, the corresponding equality equations define a tangent line through the common event point. A candidate is mechanically admissible only if one orientation of that line enters the appropriate Signorini region. The theorem below formalizes this statement: within

the regular, strictly complementary class considered here, every feasible support produces one local half-branch and every such half-branch is recovered by the support enumeration.

3.1. Supports and strict event cones

At $\mathbf{y}_e$, every event contact has $g_i = p_i = 0$. A post-event *support* $S \subseteq \mathcal{E}$ specifies which event contacts remain active:

$$\mathcal{A}_S^{\text{out}} = (\mathcal{A}^- \setminus \mathcal{E}) \cup S. \tag{8}$$

Let $N = \dim \mathbf{y} = n + 1 + m$. For each support, the outgoing equality map contains $N - 1$ equations:

$$\mathbf{F}_{\mathcal{A}_S^{\text{out}}} : U_S \subset \mathbb{R}^N \to \mathbb{R}^{N-1}, \qquad \mathbf{F}_{\mathcal{A}_S^{\text{out}}}(\mathbf{y}_e) = \mathbf{0}, \tag{9}$$

for a neighborhood U_S of $\mathbf{y}_e$. Its tangent equations are:

$$\mathbf{J}_S \mathbf{t} = \mathbf{0}, \qquad \mathbf{J}_S = D\mathbf{F}_{\mathcal{A}_S^{\text{out}}}(\mathbf{y}_e) \in \mathbb{R}^{(N-1)\times N}. \tag{10}$$

If $\operatorname{rank}\mathbf{J}_S = N - 1$, the null space is one dimensional. The two orientations of that tangent line have different mechanical meanings. Define the strict event cone:

$$\mathcal{K}_S = \{\mathbf{t} \neq \mathbf{0} : Dp_i(\mathbf{y}_e)\mathbf{t} > 0 \ (i \in S), \quad Dg_i(\mathbf{y}_e)\mathbf{t} > 0 \ (i \in \mathcal{E} \setminus S)\}. \tag{11}$$

A tangent orientation in $\mathcal{K}_S$ moves into the Signorini interior of support S.

A *regular strict Signorini half-branch* is a C^1 equilibrium curve $\gamma(s)$ defined for $0 \le s < \varepsilon$ that starts at $\mathbf{y}_e$ and has a nonzero tangent there. For all sufficiently small $s > 0$, it keeps one strict outgoing support, its outgoing Jacobian has rank $N - 1$ at the event, and its first-order event rates have the signs required by that support. Two parameterized curves represent the same *branch germ* when they trace the same punctured local curve after an orientation-preserving reparameterization.

Theorem 1 (Regular local branch decomposition). *Let $\mathcal{E} \neq \varnothing$. Assume that all non-event contact inequalities are strict at $\mathbf{y}_e$ and that, for every support $S \subseteq \mathcal{E}$, the map $\mathbf{F}_{\mathcal{A}_S^{\text{out}}} : U_S \to \mathbb{R}^{N-1}$ is C^1 near $\mathbf{y}_e$. For any support satisfying $\operatorname{rank}\mathbf{J}_S = N - 1$:*

1. *if $\ker\mathbf{J}_S \cap \mathcal{K}_S \neq \varnothing$, that intersection is exactly one oriented ray and it determines a unique local regular strict Signorini half-branch germ with support S;*
2. *if $\ker\mathbf{J}_S \cap \mathcal{K}_S = \varnothing$, no regular strict first-order half-branch with support S leaves $\mathbf{y}_e$.*

Moreover, every regular strict Signorini half-branch leaving $\mathbf{y}_e$ is generated by exactly one feasible regular support ray, and germs associated with different supports are disjoint away from $\mathbf{y}_e$ in a sufficiently small neighborhood. Consequently, conditional on the accepted corrected event state and the stated regularity assumptions, support enumeration is exhaustive for the regular, strictly complementary local Signorini half-branch germs.

Proof. For a regular support, $\ker\mathbf{J}_S$ is a line. The cone $\mathcal{K}_S$ is defined by strict homogeneous sign inequalities. Hence, if one nonzero vector $\mathbf{t}$ belongs to $\ker\mathbf{J}_S \cap \mathcal{K}_S$, every positive multiple of $\mathbf{t}$ belongs to it and every negative multiple violates the event-rate signs. The intersection is therefore exactly one oriented ray.

Choose an auxiliary phase vector $\mathbf{d}$ such that $\alpha = \mathbf{d}^T\mathbf{M}\mathbf{t} > 0$; such a choice always exists because $\mathbf{M}$ is positive definite (for example, $\mathbf{d} = \mathbf{t}$). Rescale the tangent representative as $\hat{\mathbf{t}} = \mathbf{t}/\alpha$. The bordered Jacobian:

$$\mathbf{R}\begin{bmatrix}\mathbf{J}_S \\ \mathbf{d}^T\mathbf{M}\end{bmatrix}$$

is nonsingular. Applying the implicit-function theorem to:

$$\mathbf{F}_{\mathcal{A}_S^{\text{out}}}(\mathbf{y}) = \mathbf{0}, \qquad \mathbf{d}^T\mathbf{M}(\mathbf{y} - \mathbf{y}_e) = s$$

gives a unique local curve as a set, up to an orientation-preserving reparameterization, with $\mathbf{y}'(0) = \hat{\mathbf{t}}$. For each event contact, let $\phi_i^S = p_i$ when $i \in S$ and $\phi_i^S = g_i$ when $i \in \mathcal{E} \setminus S$. Then,

$$\phi_i^S\big(\mathbf{y}(s)\big) = s\, D\phi_i^S(\mathbf{y}_e)\hat{\mathbf{t}} + o(s).$$

Positive rescaling preserves every strict event-rate sign. The selected gaps or multipliers are therefore positive for all sufficiently small $s > 0$. The strict non-event inequalities persist by continuity. The curve is a local Signorini half-branch with support S and is unique within that outgoing stratum.

Conversely, a regular strict half-branch has a fixed support for sufficiently small positive parameter. Its tangent lies in the null line of that support and satisfies the strict event signs, so it belongs to the enumerated ray. If two supports differ, at least one event contact is strictly active on one branch and strictly inactive on the other. Their germs therefore cannot coincide away from $\mathbf{y}_e$. This proves both exhaustiveness and disjointness in the stated class. □

Corollary 2 (Mirror pairing at a symmetric two-contact event). *Suppose a linear involution $\mathcal{R}$ fixes $\mathbf{y}_e$ and a contact permutation ρ satisfies, for every support S near the event, $\mathbf{F}_{\mathcal{A}_{\rho(S)}^{\text{out}}}(\mathcal{R}\mathbf{y}) = \mathbf{Q}_S\mathbf{F}_{\mathcal{A}_S^{\text{out}}}(\mathbf{y})$, with $\mathbf{Q}_S$ nonsingular, while the gap and multiplier components are permuted consistently. Then $\mathcal{R}$ maps the branch germ of support S to the branch germ of support $\rho(S)$. If two event contacts are exchanged by the reflection, the two singleton-support branches form a mirror pair.*

Proof. The stated equivariance maps the S-stratum zero set and its strict event cone to those of $\rho(S)$. Theorem 1 gives a unique branch germ for each feasible ray, so the reflected branch is the branch associated with the reflected support. □

Remark 3 (Conditional completeness). The theorem classifies regular, strictly complementary branch germs once the corrected event group is accepted. It does not certify that the event is the first exact event on the incident path, and it does not cover grazing, higher-order departure, singular strata, stability, or physical branch selection.

3.2. Interpretation and numerical checks

A support states which event contacts are active immediately after the event. Its linearized equality system gives a tangent line, and a branch in the regular strict class exists only when one orientation enters the corresponding Signorini cone. The phase row is not part of this geometric existence statement; it is used afterwards for traversal. Numerically, common-state correction defines $\mathbf{y}_e$, singular values test outgoing rank, event rates test cone feasibility, and short nonlinear restarts verify that feasible tangent rays are realized by nearby equilibrium states.

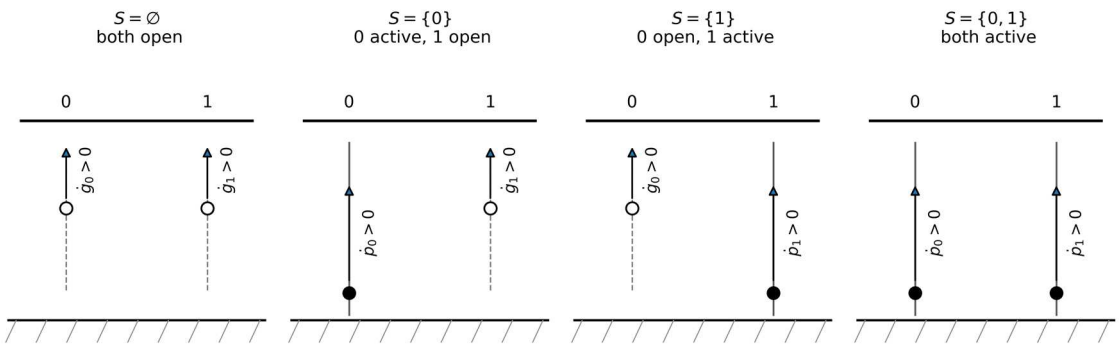


Fig. 2. A two-contact event has four supports. The theorem associates each feasible regular support ray with one local half-branch. A traversal rule is applied only after the branch geometry has been found.

3.3. Computing the support rays

The large mechanical part of the tangent system is shared by all supports. Let $\mathcal{N} = \{1, \dots, m\} \setminus \mathcal{E}$, collect the non-event variables in $\dot{\mathbf{x}} = (\dot{\mathbf{u}}, \dot{\lambda}, \dot{\mathbf{p}}_{\mathcal{N}})$, and set $\mathbf{z} = \dot{\mathbf{p}}_{\mathcal{E}}$. The square matrix $\mathbf{A} \in \mathbb{R}^{(N-|\mathcal{E}|)\times(N-|\mathcal{E}|)}$ is the phase-bordered equilibrium/non-event system, $\mathbf{C} \in \mathbb{R}^{(N-|\mathcal{E}|)\times|\mathcal{E}|}$ injects the event-multiplier rates, $\mathbf{D} \in \mathbb{R}^{|\mathcal{E}|\times(N-|\mathcal{E}|)}$ maps $\dot{\mathbf{x}}$ to event-gap rates, and $\mathbf{b}_s$ carries the phase right-hand side $s \in \{+1, -1\}$. The phase-normalized equations have the form:

$$\mathbf{A}\dot{\mathbf{x}} + \mathbf{C}\mathbf{z} = \mathbf{b}_s, \qquad \dot{\mathbf{g}}_{\mathcal{E}} = \mathbf{D}\dot{\mathbf{x}}, \qquad s \in \{+1, -1\}. \tag{12}$$

when $\mathbf{A}$ is nonsingular, one factorization gives:

$$\dot{\mathbf{g}}_{\mathcal{E}} = \mathbf{q}_s + \mathbf{H}\mathbf{z}, \qquad \mathbf{q}_s = \mathbf{D}\mathbf{A}^{-1}\mathbf{b}_s, \qquad \mathbf{H} = -\mathbf{D}\mathbf{A}^{-1}\mathbf{C}. \tag{13}$$

For a support S, the active event contacts satisfy:

$$\mathbf{H}_{SS}\mathbf{z}_S = -\mathbf{q}_{s,S}. \tag{14}$$

The remaining signs test membership in $\mathcal{K}_S$. If the common matrix is singular or poorly conditioned, the full outgoing tangent system is solved support by support. The common reduction accelerates classification; the theorem itself depends only on the outgoing strata. For $k = |\mathcal{E}|$ event contacts, however, the support loop still contains 2^k candidates. Reusing the factorization reduces the cost per candidate but does not remove this exponential growth.

Finally, the incoming tangent labels the geometric ray through:

$$\pi(\mathbf{t}) = \mathbf{c}_e^T \mathbf{M}\mathbf{t}. \tag{15}$$

Positive and negative values indicate forward and reverse traversal relative to the incident computation. They do not change the branch set established by Theorem 1. If $|\pi|$ falls below the projection tolerance, the incoming phase row does not assign a stable traversal direction. The implementation labels that case as zero projection and requires an alternative traversal row rather than forcing a forward/reverse decision. None of the 60 feasible truss rays reported below falls into this zero-projection case.

4. A symmetric Opening with Three Forward Children

4.1. Mechanical model and symmetry

To make every local choice inspectable, we use a seven-node, fourteen-bar arch with four possible vertical contacts and 15 augmented unknowns. The model is small enough to examine the corrected event state, all support choices, the associated tangent lines, and the nearby nonlinear branches directly. Figure 1(a) shows the structure, and Table 2 lists the complete definition. Contact and node labels in the benchmark are zero based; the abstract notation in Section 2 remains one based.

At B0/E27, reflection about the vertical centerline exchanges nodes $1 \leftrightarrow 5$ and $2 \leftrightarrow 4$, fixes node 3 and the load coordinate, changes the sign of horizontal displacements, preserves vertical displacements, and maps:

$$(p_0, p_1, p_2, p_3) \mapsto (p_1, p_0, p_3, p_2). \tag{16}$$

The bars, loads, clearances, incident active set, and continuation metric are invariant. The stored event state and phase row satisfy this symmetry to infinity-norm defects 9.30×10^{-16} and 8.46×10^{-17}.

4.2. Four supports and the local branch junction

At the decisive event, contacts 0 and 1 are active on the incident path and both multipliers vanish. The four possible post-event supports are $\varnothing$, $\{0\}$, $\{1\}$, and $\{0,1\}$ (see Fig. 2). Reflection fixes the empty and full supports and exchanges the singleton supports. For an exactly reflection-fixed event state, Corollary 2 therefore pairs the two singleton branches; the archived numerical state is tested against this symmetry to the floating-point defects reported above.

Table 2. Definition of the four-candidate-contact truss.

Item	Definition
Nodes	nodes 0–6: $(-3,0), (-2,0.45), (-1,0.65), (0,0.75), (1,0.65), (2,0.45), (3,0)$; nodes 1–5 are free
Bars	fan bars $(0,i)$ and $(i,6)$, $i = 1, \dots, 5$, with $EA = 1$; chords $(1,2), (2,3), (3,4), (4,5)$ with $EA = 0.15$
Vertical loads	nodal weights $0.45, 0.8, 1, 0.8, 0.45$ on nodes 1–5, multiplied by λ
Contacts	contact 0: node 2, clearance 0.5; contact 1: node 4, clearance 0.5; contact 2: node 1, clearance 0.105; contact 3: node 5, clearance 0.105
State	ten free nodal displacements, load factor, and four multipliers; 15 unknowns
Metric	unit weights on displacement and load coordinates; multiplier weights 0.05

Table 3. Support decomposition at the decisive two-contact opening. The minimum event rate is measured on the metric-unit geometric ray; $\sigma_{\min}/\sigma_{\max}$ refers to the unbordered outgoing Jacobian, and π is the incoming-phase projection.

Support S	Post-event contact status	Minimum event rate	$\sigma_{\min}/\sigma_{\max}$	π	Branch interpretation
$\varnothing$	both contacts open	6.307×10^{-1}	3.607×10^{-4}	$+0.4463$	symmetric forward child
$\{0\}$	0 active, 1 open	1.019×10^{-3}	1.437×10^{-2}	$+0.3139$	asymmetric forward child
$\{1\}$	0 open, 1 active	1.019×10^{-3}	1.437×10^{-2}	$+0.3139$	mirror-asymmetric forward child
$\{0,1\}$	both contacts active	4.856×10^{-2}	1.580×10^{-2}	-1.0000	reverse incident half-branch

Table 4. Computer-assisted event exclusion on five incoming segments. "Pre-event" is the smallest event coordinate before the terminal box; "non-event" is the smallest other contact coordinate.

Segment	Contact	Terminal event box	Minimum pre-event	Minimum non-event	Maximum contraction
B0/S27	0	$2.652645015257e-2 \ +/- \ 3.906e-9$	9.262×10^{-6}	4.796×10^{-5}	7.063×10^{-3}
B0/S27	1	$2.652645015257e-2 \ +/- \ 3.906e-9$	9.262×10^{-6}	4.796×10^{-5}	7.063×10^{-3}
B2/S14	2	$1.234290472157e-3 \ +/- \ 3.906e-9$	2.794×10^{-8}	1.236×10^{-3}	1.482×10^{-3}
B2/S47	3	$1.792758494749e-3 \ +/- \ 3.906e-9$	1.948×10^{-8}	7.306×10^{-4}	9.688×10^{-4}
B3/S14	3	$1.234290472130e-3 \ +/- \ 3.906e-9$	2.794×10^{-8}	1.236×10^{-3}	1.482×10^{-3}
B3/S47	2	$1.792758494696e-3 \ +/- \ 3.906e-9$	1.948×10^{-8}	7.306×10^{-4}	9.688×10^{-4}

All four outgoing strata have rank 14 in the 15-dimensional state space, and all four tangent lines meet their strict event cones. Theorem 1 therefore gives four local half-branch germs: the reverse incident branch and three forward children. The symmetric child corresponds to both contacts opening. The two singleton children break reflection symmetry and form the pair predicted by Corollary 2. The multiplicity is caused by the change of complementarity stratum, not by a singular tangent stiffness on any one outgoing stratum.

To display the junction, let $w_i = -u_{iy}$ be the downward vertical displacement of node i, set $w_c = w_3$, and define:

$$\eta = (w_2 - w_4)/2, \qquad \zeta = w_{c,e} - w_c. \tag{17}$$

Figure 3 projects the corrected continuation states onto (η, ζ). The incident and symmetric branches remain on the symmetry axis, while the singleton supports leave the event as a reflected pair.

4.3. Excluding earlier contact zeros on the decisive segments

Theorem 1 is conditional on the accepted event group, so event detection is checked separately. The decisive opening and four graph segments with the smallest sampled contact margins were enclosed by interval/Krawczyk path tubes [22–25]. Each segment was divided into 128 slabs. Two independent implementations were used: an outward-expanded binary64 interval calculation and a 100-decimal-digit directed-rounding replay. At the symmetric B0/E27 event, the latter also performs a symmetry-normalized cross-check; the unsymmetrized replay remains the direct check of the stored finite-precision parameterization.

All 640 slabs satisfy strict Krawczyk self-mapping tests, 635 joining boxes connect adjacent slabs, and six terminal event boxes establish opposite endpoint signs with a strictly negative signed event derivative. Table 4 reports the decisive margins. At B0/E27, independent terminal brackets for contacts 0 and 1 overlap and their midpoints differ by about 10^{-16} in the continuation parameter. Together with the common-state correction, this is symmetry-protected numerical evidence for simultaneous opening at the stated precision; it is not an exact symbolic proof. The certificate covers these five selected incoming segments, not the complete operational graph.

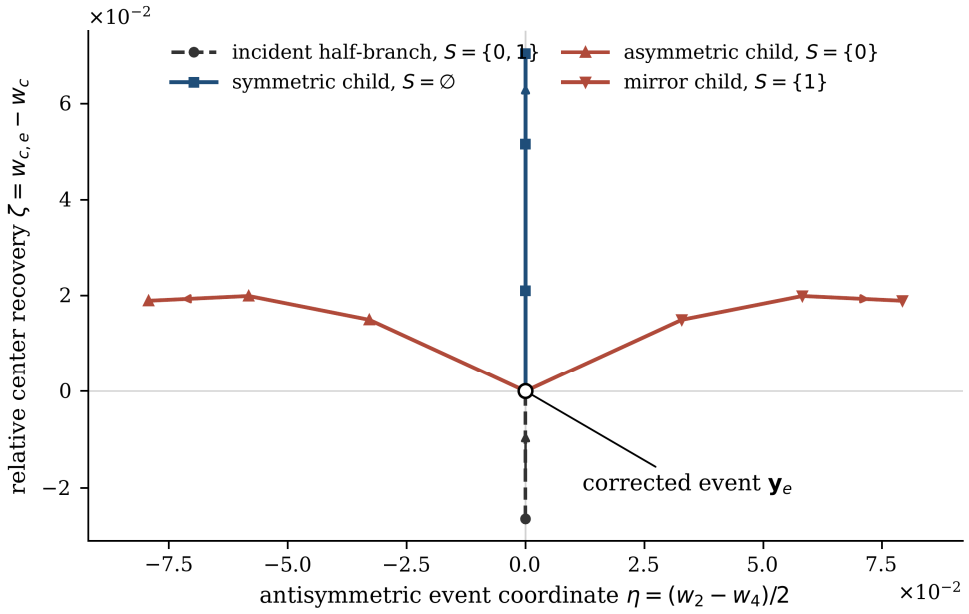


Fig. 3. Local branch geometry at the decisive opening. Markers are corrected continuation states and connecting lines guide the eye. The event is the common origin. The fully active support approaches it, the empty support gives the symmetric child, and the singleton supports give the mirror-asymmetric children.

Table 5. Five-mesh twin-pad classification. The event nodes are the nearest symmetric pair to the centerline; support mask 0 denotes $S = \varnothing$ and mask 3 denotes $S = \{0,1\}$.

Mesh	Displacement dofs	Event-node x	Separation	Event load	Support/traversal
32×2	186	± 0.3125	0.6250	7.62540e-3	0 reverse; 3 forward
48×3	376	± 0.20833	0.41667	6.12890e-3	0 reverse; 3 forward
64×4	630	± 0.15625	0.31250	5.34530e-3	0 reverse; 3 forward
80×5	948	± 0.12500	0.25000	5.11599e-3	0 reverse; 3 forward
96×6	1,330	± 0.10417	0.20833	4.90458e-3	0 reverse; 3 forward

4.4. Nonlinear checks of the branch germs

The operational graph contains 24 accepted groups and 72 support records. Sixty supports possess a feasible oriented ray: 24 with positive incoming projection and 36 with negative projection. Every feasible ray is corrected on its nonlinear outgoing stratum at phase steps 10^{-5}, 5×10^{-6}, 2.5×10^{-6}, and 1.25×10^{-6}. Negative-projection rays use a sign-adjusted phase row so that the tested orientation remains in the event cone. All 60 nonlinear corrections and secant-convergence checks pass the stated thresholds. The largest final relative metric secant error is 1.36×10^{-4}, the smallest last-two refinement order is 0.988, and the largest corrected residual is 1.44×10^{-13}.

At the two terminal openings, all four supports possess negative-projection rays and none has a positive-projection ray. Their nonlinear continuation confirms that these are orientation-selected endpoints rather than locally isolated equilibria. Across 13 multistart runs and 400 initial points, an analytic-Jacobian search and a separately assembled finite-difference-Jacobian Fischer–Burmeister sphere search recover the incident branch and the same three forward children at B0/E27; no additional converged branch is observed. These searches are corroborative, not a completeness proof. Conditional completeness follows from Theorem 1 and the verified support assumptions.

5. Engineering Transfer to a Sparse Finite-Element Strip

Figure 1(b) shows the twin-pad transfer benchmark. The shallow parabolic strip has nondimensional length 10, rise 0.60, in-plane thickness 0.60 and unit out-of-plane thickness. Total-Lagrangian T3 elements are used in plane stress with a Saint-Venant–Kirchhoff material, $E = 1$ and $\nu = 0.30$. Both ends are fixed. A downward line load on the upper boundary is normalized to unit resultant. Candidate lower-boundary nodes satisfy $0.05 \le |x| \le 2.6$ and contact the rigid plane $y = -0.55$ with fixed vertical normals.

Five meshes, from 186 to 1,330 displacement degrees of freedom, retain the same discrete support classification: the fully closed support $S = \{0,1\}$ is the sole forward child, the fully open support is a reverse ray, and the singleton supports are cone infeasible. Reduced and direct tangent calculations agree within the stated tolerances.

The event-node separation is exactly $2h_x$ and decreases under refinement, but the event load changes from 7.62540e-3 to 4.90458e-3. No convergence rate or mesh-uniform conditioning bound is established. The calculation therefore demonstrates portability of the corrected-event/support-classification machinery to sparse finite-element assembly; it does not establish continuum convergence, two distinct continuum contact points, or continuum-generated forward multiplicity.

A separate 66-record perturbation study probes the numerical definition of simultaneity on two meshes. Antisymmetric clearance offsets from 10^{-4} to 10^{-13} are combined with event tolerances 2×10^{-8}, 2×10^{-10} and 2×10^{-12}. The outcomes are 6 symmetry-protected baseline cases, 40 resolved sequential events, 8 unresolved tolerance overlaps and 12 tolerance-merged cases. In the merged cases, the accepted state is interpreted as belonging to a nearby clearance-perturbed problem rather than as an exact simultaneous event of the asymmetric model; the maximum componentwise clearance backward error is 2.00×10^{-12}. This makes simultaneity a controlled finite-resolution policy rather than a claim of exact coincidence under arbitrary perturbations.

6. Discussion and Conclusions

Three decisions are deliberately kept apart in the proposed procedure. The nonlinear corrector fixes the common event state. Support classification then determines which regular strict branches leave that state. Only afterwards does the continuation phase label the corresponding rays as forward or reverse. At the decisive two-contact opening, all four supports are regular and feasible: three rays point forward - one symmetric and two mirror-asymmetric - while the fully active support is the reverse half of the incident branch. Short nonlinear restarts recover each feasible ray as an actual nearby equilibrium branch. The claims are intentionally local and conditional. The standard implicit-function theorem supplies local smoothness on each regular outgoing stratum; the contribution is the support-indexed decomposition and its integration with corrected event localization and continuation bookkeeping. Exhaustive support enumeration requires 2^k candidates for a k-contact event. This is transparent for the one- and two-contact groups studied here, but it is not a scalable strategy for large simultaneous groups. Grazing, singular strata, friction, changing normals, higher-order departure and continuum-generated multibranch contact remain outside the present result. The finite-element example has a more modest role. It shows that the low-dimensional event calculation can be attached to a sparse assembled mechanical system without changing the classifier; it does not establish continuum convergence. Taken together with the truss results and the stated regularity assumptions, the computations support the main conclusion: once a corrected regular Signorini event has been accepted, the feasible complementary support rays account for exactly the regular, strictly complementary local half-branch germs covered by Theorem 1.

Author Contributions

M. Hamdaoui contributed to the Conceptualization, Methodology, Software, Validation, Formal analysis, Investigation, Data curation, Visualization, Writing–original draft, and Writing–review and editing. The author discussed the results, reviewed, and approved the final version of the manuscript.

Acknowledgments

Not applicable.



Conflict of Interest

The author declares that he has no known competing financial interests or personal relationships that could have appeared to influence the work reported in this paper.

Funding

Not applicable.

Data Availability Statements

The numerical data supporting the results reported in this article are supplied with the revised submission in the accompanying data-only archive, provided as CSV and TXT files. The source code and implementation scripts are available from the corresponding author upon reasonable request.

References

[1] Cochelin, B., A path-following technique via an asymptotic-numerical method, *Computers & Structures*, 53(5), 1994, 1181–1192.
[2] Cochelin, B., Damil, N., Potier-Ferry, M., Asymptotic-numerical methods and Padé approximants for non-linear elastic structures, *International Journal for Numerical Methods in Engineering*, 37(7), 1994, 1187–1213.
[3] Najah, A., Cochelin, B., Damil, N., Potier-Ferry, M., A critical review of asymptotic numerical methods, *Archives of Computational Methods in Engineering*, 5, 1998, 31–50.
[4] Aggoune, W., Zahrouni, H., Potier-Ferry, M., High-order prediction–correction algorithms for unilateral contact problems, *Journal of Computational and Applied Mathematics*, 168, 2004, 1–9.
[5] Aggoune, W., Zahrouni, H., Potier-Ferry, M., Asymptotic numerical methods for unilateral contact, *International Journal for Numerical Methods in Engineering*, 68(6), 2006, 605–631.
[6] Lejeune, A., Boudaoud, H., Potier-Ferry, M., Charpentier, I., Zahrouni, H., Automatic solver for non-linear partial differential equations with implicit local laws: Application to unilateral contact, *International Journal for Numerical Methods in Engineering*, 94(9), 2013, 850–867.
[7] Wriggers, P., Wagner, W., Stein, E., Algorithms for non-linear contact constraints with application to stability problems of rods and shells, *Computational Mechanics*, 2(3), 1987, 215–230.
[8] Stein, E., Wagner, W., Wriggers, P., Nonlinear stability-analysis of shell and contact-problems including branch-switching, *Computational Mechanics*, 5, 1990, 428–446.
[9] Björkman, G., Path following and critical points for contact problems, *Computational Mechanics*, 10, 1992, 231–246.
[10] Schulz, M., Pellegrino, S., Equilibrium paths of mechanical systems with unilateral constraints. I. Theory, *Proceedings of the Royal Society of London. Series A: Mathematical, Physical and Engineering Sciences*, 456, 2000, 2223–2242.
[11] Ligurský, T., Renard, Y., A continuation problem for computing solutions of discretised evolution problems with application to plane quasi-static contact problems with friction, *Computer Methods in Applied Mechanics and Engineering*, 280, 2014, 222–262.
[12] Ligurský, T., Renard, Y., Bifurcations in piecewise-smooth steady-state problems: Abstract study and application to plane contact problems with friction, *Computational Mechanics*, 56(1), 2015, 39–62.
[13] Ligurský, T., Renard, Y., A method of piecewise-smooth numerical branching, *ZAMM – Journal of Applied Mathematics and Mechanics*, 97(7), 2017, 815–827.
[14] Kubatschek, T., Förster, A., Investigation of existing and new approaches to step size control in a continuation framework, *Computers & Structures*, 313, 2025, 107747.
[15] Rey, V., On the influence of resolution algorithm's parameters on the converged solution for a Coulomb friction contact problem exhibiting multiple solutions, *Comptes Rendus Mécanique*, 354, 2026, 461–480.
[16] El Khalfi, H., Baiz, O., Benaissa, H., Error estimates of piezoelectric Signorini's contact problems, *ZAMM – Journal of Applied Mathematics and Mechanics*, 103(12), 2023, e202300112.
[17] El Khalfi, H., Faiz, Z., Baiz, O., Benaissa, H., Error estimates of unilateral piezoelectric contact problem in a curved and smooth boundary domain, *Mathematical Methods in the Applied Sciences*, 48(1), 2025, 779–803.
[18] El Khalfi, H., Faiz, Z., Baiz, O., Benaissa, H., Optimal convergence of thermoelastic contact problem involving nonlinear Hencky-type materials with friction conditions, *Iranian Journal of Science*, 49(7), 2025, 133–149
[19] El Khalfi, H., Faiz, Z., Oultou, A., Benaissa, H., Error analysis of a frictional piezoelectric contact problem, *Acta Applicandae Mathematicae*, 201(1), 2026, 14.
[20] El Khalfi, H., Benaissa, H., Penalization of Coulomb's frictional Signorini's contact problem for locking piezoelectric materials, *Rendiconti del Circolo Matematico di Palermo Series 2*, 74(4), 2025, 127.
[21] El Khalfi, H., Benaissa, H., Finite element analysis of a thermo-electro-elastic Lamé system with penalized contact conditions, *Zeitschrift für Analysis und ihre Anwendungen*, 2026, DOI: 10.4171/ZAA/1834.
[22] Moore, R.E., Kearfott, R.B., Cloud, M.J., *Introduction to Interval Analysis*, SIAM, Philadelphia, 2009.
[23] Rump, S.M., Verification methods: Rigorous results using floating-point arithmetic, *Acta Numerica*, 19, 2010, 287–449.
[24] Duff, T., Lee, K., Certified homotopy tracking using the Krawczyk method, *Proceedings of the 2024 international symposium on symbolic and algebraic computation*, 2024, 274–282.
[25] Guillemot, A., Lairez, P., Validated numerics for algebraic path tracking, *Proceedings of the 2024 international symposium on symbolic and algebraic computation*, 2024, 36–45.

ORCID iD

Mohamed Hamdaoui https://orcid.org/0000-0003-3315-7373

© 2026 Shahid Chamran University of Ahvaz, Ahvaz, Iran. This article is an open access article distributed under the terms and conditions of the Creative Commons Attribution-NonCommercial 4.0 International (CC BY-NC 4.0 license) (http://creativecommons.org/licenses/by-nc/4.0/).

How to cite this article: Hamdaoui M. Event-Driven Asymptotic Continuation and Regular Branch Decomposition for Signorini Contact, *J. Appl. Comput. Mech.*, xx(x), 2026, 1–8. https://doi.org/10.22055/jacm.2026.49691.6165

Publisher's Note Shahid Chamran University of Ahvaz remains neutral with regard to jurisdictional claims in published maps and institutional affiliations.